Transient Control of the Reactive Current for the Line-Side Converter of the Brushless Doubly-Fed Induction Generator in Stand-Alone Operation

Xingwei Wang, *Student Member, IEEE*, Hua Lin, *Member, IEEE*, and Zhe Wang

***Abstract*—In this paper, the transient control algorithm of the reactive current by the line-side converter (LSC) control is proposed when the inductive load is suddenly connected or disconnected from the stator power winding (PW) of the brushless doubly-fed induction generator. In stand-alone operation, the quality of the voltage waveform at the point-of-common coupling (PCC) will be strongly affected due to the reactive power change of load. Moreover, when the amplitude of the PCC voltage is higher than the dc-link voltage, the LSC cannot work normally. To tackle this problem, many control strategies, such as predictive current control, direct voltage control, etc., are usually developed in the machine-side converter to supply the reactive power, but the LSC can also assist in stabilizing the PCC voltage fluctuation by supplying or absorbing reactive current. This paper analyzes the transient state of the load current and the PCC voltage when the load is suddenly connected to the stator PW, and proposes a compensation algorithm which has a good transient-state performance. Then, the controllability of the LSC during the PCC voltage swell is analyzed when the load is disconnected from the stator PW. A high-voltage ride-through control strategy is proposed by using the reactive current of the LSC. The correctness of the proposed method is demonstrated by simulations and experiments.**

***Index Terms*—Brushless doubly-fed induction generator (BDFIG), reactive current compensation, stand-alone operation, transient response.**

NOMENCLATURE

u_{sp}, u_{sc}	Stator PW and stator CW voltage.
i_{sp}, i_{sc}, i_r	Stator PW, stator CW, and rotor current.
P_{sp}, P_{sc}	Stator PW and stator CW power.
R_{sp}, R_{sc}, R_r	Stator PW, stator CW, and rotor resistance.
L_{spm}, L_{rpm}	Stator PW and rotor coupling inductance.
L_{scm}, L_{rcm}	Stator CW and rotor coupling inductance.
$L_{sp\sigma}$, $L_{sc\sigma}$, $L_{r\sigma}$	Stator PW, stator CW, and rotor leakage inductance.
L_s, R_s	Filter inductance and inner resistance.
ω_p, ω_c, ω_r	Stator PW, stator CW, and rotor angular speed.
e_{sp}, e_{sc}	Stator PW and stator CW induced electromotive force.
v	AC-side voltage of the LSC.
u	Stator PW output voltage at the PCC.
i, i_L	Input current of the LSC and load current.
p_p, p_c	Stator PW and stator CW pole pairs.
u_{dc}	DC-link voltage.
Superscripts	
*	Reference value.
Subscripts	
sp, sc, r	Stator PW, stator CW, and rator.
a, b, c	a-phase, b-phase, and c-phase.
d, q	Synchronous rotating dq axis.
α, β	Stationary $\alpha\beta$ axis.

Manuscript received January 28, 2016; revised April 26, 2016 and July 14, 2016; accepted September 11, 2016. Date of publication September 24, 2016; date of current version May 9, 2017. This work was supported in part by the Power Electronics Science and Education Development Program of Delta Environmental and Educational Foundation under Grant DREM2015001. Recommended for publication by Associate Editor A. Mertens. *(Corresponding author: Hua Lin.)*

The authors are with the State Key Laboratory of Advanced Electromagnetic Engineering and Technology, Huazhong University of Science and Technology, Wuhan 430074, China (e-mail: wxw@mail.hust.edu.cn; lhua@mail.hust.edu.cn; ranger_wong@foxmail.com).

Color versions of one or more of the figures in this paper are available online at http://ieeexplore.ieee.org.

Digital Object Identifier 10.1109/TPEL.2016.2609461

I. INTRODUCTION

BRUSHLESS doubly-fed induction generator (BDFIG) is a new type of induction machine which has the advantages of DFIG that it only requires a low-power rating of the converter compared to the nominal power of the machine. Furthermore, the absence of brush gear and slip rings in the BDFIG can increase the system reliability and decrease the high maintenance costs [1]. With the independent control of the active and reactive power, the BDFIG as a stand-alone power generation has a wide application of variable-speed constant-frequency generator in some embedded generation systems, such as ship shaft generation systems [2], [3].

The BDFIG has two sets of three-phase stator windings. One is the stator power winding (PW) which is used for generating power and connected to the load, the other set of stator windings, called the stator control winding (CW), is supplied with a variable voltage and frequency power converter which is also connected to the stator PW [4]. The rotor winding (RW) is used to couple to the two stator windings. In the stand-alone BDFIG system, the generator should be controlled to build up a constant stator PW voltage to support the loads, but the voltage at the point-of-common coupling (PCC) will fluctuate in case of larger variations of the loads. Especially, the load is connected or disconnected from the PCC. The voltage fluctuation degrades the

performance of other loads connected to the PCC and introduces torque pulsations [5].

The associated converter is composed of two back-to-back voltage-source converters with a common dc-link. Usually the machine-side converter (MSC) controls the stator CW current directly. Then, the output voltage of the stator PW can be regulated indirectly, and the line-side converter (LSC) is used to control the dc-link voltage regardless of power flow direction through the MSC [6]. The LSC can also assist in stabilizing the PCC voltage fluctuation by supplying or absorbing the reactive current. In case the inductive load is connected to the stator PW of the BDFIG, the system will generate reactive power for the load. The disadvantage of reactive power compensation based on the MSC control is the slower response compared to the LSC control because of the larger mechanical inertia. Since one end of the LSC is connected with the PCC and the other end is connected with the dc-link capacitor, the control bandwidth of the LSC is significantly higher than that of the BDFIG. So the LSC can quickly suppress the voltage fluctuation at the PCC by producing the reactive current. In addition, based on the compensation by the MSC control, the excitation current in the stator CW will also increase to supply more reactive power when the inductive loads are connected to the PCC. So it will cause more losses and reduce the efficiency of the system [7].

Based on the reactive current compensation by the LSC control, the reactive current in the LSC is injected at the PCC by using the proportional-integral (PI) controller [8]. Implementing the PCC voltage-oriented reference frame, the q-axis current can be used to control the reactive current of the LSC. The q-axis reference value is usually calculated according to the reactive component of the load current. This conventional control scheme can result in a good steady-state performance and can be easy to implement, but in the transient period of inductive load connecting to the PCC, the reactive component of the load current may not be a constant value. Because of narrow control bandwidth of the PI controller [9], if this reactive load current is directly used as the q-axis reference value, it is impossible to obtain accurate control for the oscillation quantities. This will make the PCC voltage fluctuation more serious for a long time.

Another, when the load is disconnected from the stator PW, the PCC voltage will swell. Moreover, when the amplitude of the PCC voltage is higher than the dc-link voltage, the LSC cannot work normally [10]. Some methods employ extra sets of hardware appliances, such as the super conducting magnetic energy storage, the dynamic voltage restorer, and the static synchronous compensator (STATCOM), to suppress the voltage swell [11]–[13], but these methods would lead to higher costs and more complex design of the system.

The high-voltage ride-through (HVRT) control for the LSC itself is proposed with adaptive adjustment of the dc-link voltage reference according to the PCC voltage or supplying the reactive current to the load [14], [15]. In order to ensure the normal operation of the LSC, the dc-link voltage which is controlled as a constant under normal operation is set to a relatively high value during grid voltage swell in [14]. However, a higher dc-link voltage means that the maximum permissible voltage of the dc-link capacitors and the power semiconductor devices will increase [14]. In [15], the reactive current of the LSC is controlled on the basis of ensuring its active current control, but the relationship between the control voltage and the reactive current in the LSC is not analyzed in-depth for a given capacity constraints.

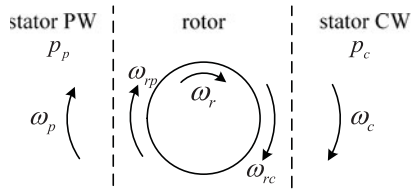

Fig. 1. BDFIG doubly-fed mode.

According to the above analysis, the transient control algorithm of the reactive current by the LSC control is proposed in case the inductive load is suddenly connected and disconnected from the stator PW. First, the voltage drop at the PCC is analyzed using the equivalent circuit for the stand-alone BDFIG system under sudden load change. Then, the transient reactive current compensation method is proposed based on the conventional PI controller. In case of the large load disconnected from the PCC, the voltage swell is analyzed and the control method of the reactive current of LSC is given to ensure the normal operation of the LSC. Lastly, the influence of this reactive current compensation on the dynamic performance of the dc-link voltage is also analyzed. Test results during steady state and transient operating conditions are presented to demonstrate the properties and correctness of the proposed method.

II. Basic Principle and Configuration of the BDFIG

The BDFIG comprises two electrically separated stator windings, called the stator PW and stator CW. The stator PW produces a p_p pole-pair field rotating at speed of ω_p and the stator CW produces a p_c pole-pair field rotating at speed of ω_c [16]. The RW is specially designed to couple to the two stator windings. The BDFIG is normally operated in the synchronous mode, called doubly-fed mode as well, as shown in Fig. 1 [3].

In Fig. 1, the RW will produce the induced current of angular speed ω_{rp} and ω_{rc} in response to the stator PW and stator CW. The angular speeds in the rotor reference frame are

$$\begin{aligned} \omega_{rp} &= \omega_p - p_p\omega_r \\ \omega_{rc} &= \omega_c - p_c\omega_r. \end{aligned} \tag{1}$$

For the only one set of RW is through the same current, it is required that $\omega_{rp} = -\omega_{rc}$. Then, the shaft angular speed ω_r is expressed by

$$\omega_r = \frac{\omega_p + \omega_c}{p_p + p_c} \tag{2}$$

where ω_p and ω_c are the angular speed of the stator PW and the stator CW, respectively.

From (2), it can be seen that with the variable speed ω_r of the BDFIG, ω_p can be kept constant by controlling ω_c. It is the operation principle of the BDFIG. When the angular speed of the stator CW is zero, the shaft angular speed ω_r is given by

$$\omega_n = \frac{\omega_p}{p_p + p_c}. \tag{3}$$

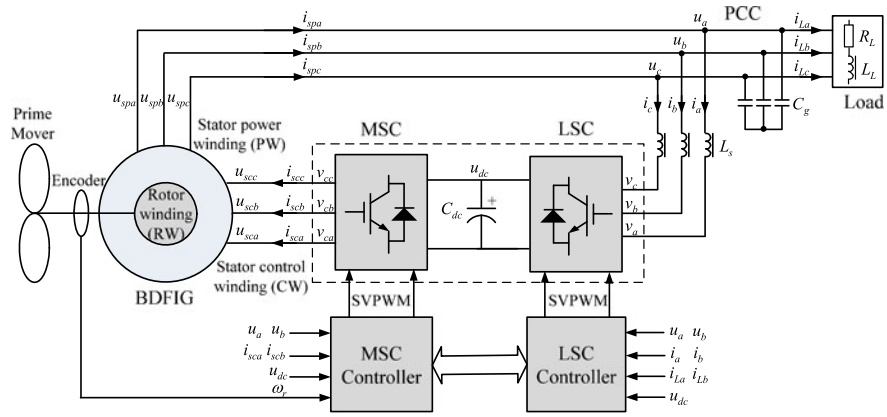

Fig. 2. Configuration of the stand-alone BDFIG system feeding resistive–inductive load.

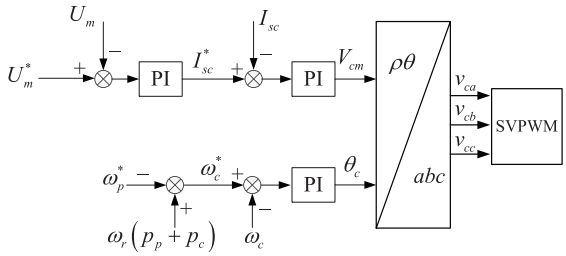

Fig. 3. Scalar control diagram of the BDFIG.

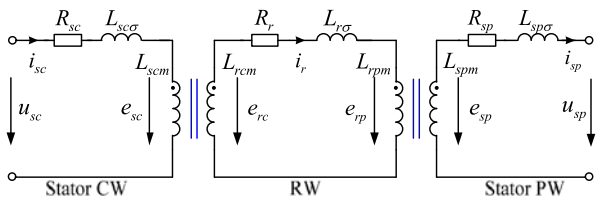

Fig. 4. Per-phase steady-state equivalent circuit of the BDFIG.

This speed is called the natural speed, and the stator CW will be fed with a dc source.

Fig. 2 shows the structure diagram of the stand-alone BDFIG system which feeds the three-phase resistive–inductive load. In Fig. 2, the stator PW is connected directly to the load and also supplies the power to the converter in stand-alone operation. The stator CW is supplied with two back-to-back converters composed of the MSC and the LSC. The converters are with a common dc-link and are also connected to the stator PW at the PCC.

In Fig. 2, a Y-connected filtering capacitor C_g is equipped with the output of the stator PW of the BDFIG. This capacitor can reduce the ripples in the stator PW voltage and filter out the harmonics produced by the LSC which works under the pulse width modulation (PWM) control method [17]. The three-phase asynchronous motor which is controlled by the Siemens inverter is used to emulate variable-speed operation of prime movers. L_L and R_L are the equivalent inductance and resistance of the load, respectively.

Usually, the MSC is used to control the stator CW current so as to regulate the voltage of the stator PW. The focus of this paper is the reactive current control of the LSC, so the scalar control scheme is used for the BDFIG in the control of the MSC based on (2), shown in Fig. 3 [18].

In Fig. 3, U_m is the amplitude of the PCC voltage u and I_{sc} is the amplitude of the stator CW current i_{sc}. V_{cm} and θ_c are the amplitude of the phase voltage v_c and phase angle of the MSC, respectively. When the amplitude of the PCC voltage is smaller than the reference value, the stator CW current will increase and vice versa. It is the simple and reliable control method for the BDFIG and avoids identifying motor parameters. This method is sufficient for low-performance drive applications, like fans and pumps.

III. Transient Reactive Current Compensation Method in Case of the Inductive Load Connection

A. Transient Analysis of the Voltage Drop in Case of the Inductive Load Connection

With the help of the equivalent circuit of the BDFIG, the operating conditions of the BDFIG and its associated converters can be obtained quickly. Fig. 4 shows a per-phase steady-state equivalent circuit of the BDFIG [16].

So the stator PW side circuit is equivalent to the combination of induced electromotive force denoted by e_{sp} and stator PW resistance and leakage inductance denoted by R_{sp} and $L_{sp\sigma}$, respectively.

In the BDFIG neglecting losses, the expressions for the power balance is given by $P_{sc} = s_b P_{sp}$ [19]. s_b is the total slip of the BDFIG. Supposed that the LSC is operated under unity power factor, the relationship between a-phase current i_a of the LSC and a-phase output current of the stator PW i_{spa} can be written as

$$i_a = s_b i_{spa} \cos\theta_p \tag{4}$$

where θ_p is the power factor angle of the stator PW. Then, the LSC can be seen as a controlled current source. Since the LSC and MSC are with a common capacitive dc-link and can be decoupled by the capacitance C_{dc}, the MSC is not considered in the circuit for LSC analysis. The a-phase equivalent circuit for the stand-alone BDFIG system seen from the stator PW side is shown in Fig. 5. In Fig. 5, i_{La} is the a-phase load current and u_a is the a-phase PCC voltage.

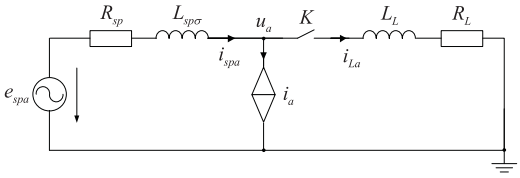

Fig. 5. a-phase equivalent circuit of the stand-alone BDFIG system.

Taking the initial angle of a-phase voltage as the reference angle, e_{spa} in time domain is described as follows:

$$e_{spa}(t) = U_m \cos(\omega t) \tag{5}$$

where U_m and ω are the amplitude of the phase voltage and angular frequency, respectively.

Then, e_{spa} in complex frequency domain can be deduced by the Laplace transformation

$$e_{spa}(s) = \frac{U_m s}{s^2 + \omega^2}. \tag{6}$$

For simplification of analysis, the BDFIG is supposed to operate at the natural speed, that is, $s_b = 0$. So a-phase current i_a of the LSC is zero, then the stator PW current i_{spa} and the load current i_{La} are equal.

Therefore, the stator PW current i_{spa} in complex frequency domain can be drawn as

$$i_{spa}(s) = \frac{e_{spa}(s)}{Ls + R} = \frac{U_m s}{(s^2 + \omega^2)(Ls + R)} \tag{7}$$

where L is the total inductance, and R is the total resistance as

$$\begin{aligned} R &= R_L + R_{sp} \\ L &= L_L + L_{sp\sigma}. \end{aligned} \tag{8}$$

If the magnitude and the angle of the total impedance are defined as following:

$$|Z| = \sqrt{R^2 + (\omega L)^2}, \quad \phi = \arctan\left(\frac{\omega L}{R}\right). \tag{9}$$

Then, (7) can be changed as

$$\begin{aligned} i_{spa}(s) &= \frac{U_m}{|Z|^2}\left(\frac{Rs}{s^2+\omega^2} + \frac{\omega^2 L}{s^2+\omega^2} - \frac{RL}{Ls + R}\right) \\ &= \frac{U_m}{|Z|}\left(\frac{s\cos\phi}{s^2+\omega^2} + \frac{\omega\sin\phi}{s^2+\omega^2} - \frac{\cos\phi}{s + \frac{R}{L}}\right). \end{aligned} \tag{10}$$

When the load is suddenly connected to the PCC, the stator PW current i_{spa} in time domain can be deduced by the inverse Laplace transformation

$$i_{spa}(t) = \frac{U_m}{|Z|}\cos(\omega t - \phi) - \frac{U_m \cos(-\phi)}{|Z|} e^{-\frac{R}{L}t}. \tag{11}$$

It can be found that the stator PW current i_{spa} contains a fundamental frequency component and a dc component in exponentially decaying. Then, i_{spb} and i_{spc} can be obtained in the same way.

The stator PW current is transformed into synchronous reference frame quantities by using the Park matrix. Then, the instantaneous active current i_{spd} and the instantaneous reactive current i_{spq} can be drawn as

$$\begin{aligned} i_{spd}(t) &= i_{spds} + i_{spdt} = \frac{U_m}{|Z|}\cos\phi - \frac{U_m \cos(\omega t + \phi)}{|Z|} e^{-\frac{R}{L}t} \\ i_{spq}(t) &= i_{spqs} + i_{spqt} = -\frac{U_m}{|Z|}\sin\phi + \frac{U_m \sin(\omega t + \phi)}{|Z|} e^{-\frac{R}{L}t} \end{aligned} \tag{12}$$

where

$$\begin{aligned} i_{spds} &= \frac{U_m}{|Z|}\cos\phi, \quad i_{spdt} = -\frac{U_m \cos(\omega t + \phi)}{|Z|} e^{-\frac{R}{L}t} \\ i_{spqs} &= -\frac{U_m}{|Z|}\sin\phi, \quad i_{spqt} = \frac{U_m \sin(\omega t + \phi)}{|Z|} e^{-\frac{R}{L}t}. \end{aligned}$$

As shown in (12), the active and reactive PW currents also contain a steady component i_{sps} which is a dc value and a transient component i_{spt} which is a decaying fundamental value in exponential form, and the steady component is exactly the positive-sequence fundamental component of the load current i_L in the dq axis.

The PCC voltage u in the synchronous qd axis reference frame is determined based on Fig. 5 as

$$\begin{aligned} u_d &= e_{spd} - R_{sp} i_{spd} - L_{sp\sigma}\frac{di_{spd}}{dt} + \omega L_{sp\sigma} i_{spq} \\ u_q &= e_{spq} - R_{sp} i_{spq} - L_{sp\sigma}\frac{di_{spq}}{dt} - \omega L_{sp\sigma} i_{spd}. \end{aligned} \tag{13}$$

So this stator PW current may cause the voltage drop and distortion at the PCC, and the voltage drop Δu in the qd axis can be expressed as

$$\begin{aligned} \Delta u_d &= R_{sp} i_{spd} + L_{sp\sigma}\frac{di_{spd}}{dt} - \omega L_{sp\sigma} i_{spq} \\ \Delta u_q &= R_{sp} i_{spq} + L_{sp\sigma}\frac{di_{spq}}{dt} + \omega L_{sp\sigma} i_{spd}. \end{aligned} \tag{14}$$

Substituting (12) into (14), (14) can be written as

$$\begin{aligned} \Delta u_d &= R_{sp}(i_{spds} + i_{spdt}) + L_{sp\sigma}\left(\omega i_{spqt} - \frac{R}{L} i_{spdt}\right) \\ &\quad - \omega L_{sp\sigma}(i_{spqs} + i_{spqt}) \\ \Delta u_q &= R_{sp}(i_{spqs} + i_{spqt}) + L_{sp\sigma}\left(-\omega i_{spdt} - \frac{R}{L} i_{spqt}\right) \\ &\quad + \omega L_{sp\sigma}(i_{spds} + i_{spdt}). \end{aligned} \tag{15}$$

Then, this equation can be simplified further

$$\begin{aligned} \Delta u_d &= (R_{sp} i_{spds} - \omega L_{sp\sigma} i_{spqs}) + \frac{R_{sp} L - L_{sp\sigma} R}{L} i_{spdt} \\ \Delta u_q &= (R_{sp} i_{spqs} + \omega L_{sp\sigma} i_{spds}) + \frac{R_{sp} L - L_{sp\sigma} R}{L} i_{spqt}. \end{aligned} \tag{16}$$

Then, a-phase voltage drop at the PCC voltage Δu_a can be deduced by the Park inverse transformation as

$$\Delta u_a = \Delta u_d \cos\omega t - \Delta u_q \sin\omega t. \tag{17}$$

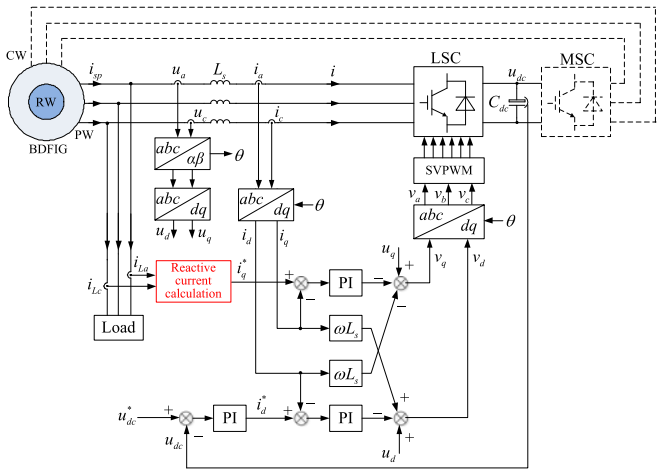

Fig. 6. Control diagram of the LSC with reactive current compensation principle.

Substituting (16) into (17), (17) can be written as

$$\begin{aligned}\Delta u_a =& \sqrt{\left(R_{sp}i_{spds}-\omega L_{sp\sigma}i_{spqs}\right)^2+\left(R_{sp}i_{spqs}+\omega L_{sp\sigma}i_{spds}\right)^2}\\ &\times\cos\left(\omega t+\varphi\right)\\ &+\frac{R_{sp}L-L_{sp\sigma}R}{L}\left(i_{spdt}\cos\omega t-i_{spqt}\sin\omega t\right)\\ =&\sqrt{\left(R_{sp}^2+\omega^2L_{sp\sigma}^2\right)\left(i_{spds}^2+i_{spqs}^2\right)}\cos\left(\omega t+\varphi\right)\\ &+\frac{R_{sp}L-L_{sp\sigma}R}{L}\left(i_{spdt}\cos\omega t-i_{spqt}\sin\omega t\right)\\ =&\frac{U_m}{|Z|}|Z_{sp}|\cos\left(\omega t+\varphi\right)-\frac{U_m}{|Z|}\frac{R_{sp}L-L_{sp\sigma}R}{L}\cos\phi e^{-\frac{R}{L}t}\end{aligned} \tag{18}$$

where

$$\varphi=\arctan\frac{-R_{sp}\omega L+\omega L_{sp\sigma}R}{R_{sp}R+\omega^2L_{sp\sigma}L},\ |Z_{sp}|=\sqrt{R_{sp}^2+\omega^2L_{sp\sigma}^2}.$$

From (18), the steady-state component of the stator PW current will cause the voltage drop and the transient component of the stator PW current will cause the voltage distorted at the PCC.

B. Transient Reactive Current Compensation by LSC Based on V–I Doubly Closed Loop

Both the LSC and the stator PW can supply the reactive power to the load. With the higher control bandwidth of the LSC, the LSC can quickly respond to the change of the PCC voltage. So it is easier and more reliable to choose the LSC to compensate the reactive current of the load.

Implementing the PCC voltage-oriented reference frame, the control scheme of the LSC adopts the voltage and current double closed-loop structure shown in Fig. 6 [20]. In Fig. 6, the phase angle θ for the coordinate transformation is calculated by the single synchronous reference frame software phase-locked loop [21]. With the conventional PI controller, the output of the voltage loop is given as the d-axis reference current to control the dc-link voltage, and the negative reactive component of the load current i_{Lq} is given as the q-axis reference current to compensate for reactive stator PW current caused by load.

When the inductive load is connected to the stator PW of the BDFIG, the reactive current of the load is calculated according to the classic instantaneous reactive power (IRP) theory. Then, the LSC will supply the reactive current to the load assisting in stabilizing the PCC voltage fluctuation.

C. Fully Reactive Current Compensation Method in Case of the Inductive Load Connection

When the BDFIG is supposed to operate at the natural speed, then the stator PW current and the load current are equal. So the reactive current of the load is

$$i_{Lq}=i_{Lqs}+i_{Lqt}=-\frac{U_m}{|Z|}\sin\phi+\frac{U_m\sin\left(\omega t+\phi\right)}{|Z|}e^{-\frac{R}{L}t} \tag{19}$$

where

$$i_{Lqs}=-\frac{U_m}{|Z|}\sin\phi,\quad i_{Lqt}=\frac{U_m\sin\left(\omega t+\phi\right)}{|Z|}e^{-\frac{R}{L}t}.$$

If the LSC is controlled to fully compensate reactive current of the load, including the steady-state component i_{Lqs} and transient component i_{Lqt}, then the whole components of the load current i_{Lq} are used as the q-axis current reference of the LSC. That is

$$i_q^*=-i_{Lq}=-i_{Lqs}-i_{Lqt}. \tag{20}$$

Then, the stator PW current does not contain the reactive component any more. So the reactive component in the stator PW current is zero, that is, $i_{spqs}=i_{spqt}=0$. The drop of the PCC voltage Δu can be deduced as

$$\begin{aligned}\Delta u_d&=R_{sp}i_{spds}+\frac{R_{sp}L-L_{sp\sigma}R}{L}i_{spdt}\\ \Delta u_q&=\omega L_{sp\sigma}i_{spds}.\end{aligned} \tag{21}$$

According to (18), the drop of the PCC voltage Δu_a is

$$\begin{aligned}\Delta u_a=&\sqrt{\left(R_{sp}^2+\omega^2L_{sp\sigma}^2\right)i_{spds}^2}\cos\left(\omega t+\varphi\right)\\ &+\frac{R_{sp}L-L_{sp\sigma}R}{L}i_{spdt}\cos\omega t\\ =&\frac{U_m}{|Z|}|Z_{sp}|\cos\phi\cos\left(\omega t+\varphi\right)\\ &-\frac{U_m}{|Z|}\frac{R_{sp}L-L_{sp\sigma}R}{L}e^{-\frac{R}{L}t}\\ &\times\left[\frac{1}{2}\cos\left(2\omega t+\phi\right)+\frac{1}{2}\cos\phi\right].\end{aligned} \tag{22}$$

It can be seen that if the reactive stator PW current is fully compensated by using the control algorithm of the LSC, the steady state of the voltage drop at the PCC has been decreased because of $\cos\phi<1$. The load inductance is bigger, the steady state of the voltage drop is smaller, but there will be double fundamental-frequency component in the voltage at the PCC,

and this component is larger than the fundamental-frequency component.

The main reason for this phenomenon is that the stator PW current still contains the transient active component i_{spdt} when the reactive current of the load is fully compensated. From (21), it can be seen that there will be an asymmetry of the transient component in the *d*-axis and the *q*-axis voltage drop. Then, a worse quality of *a*-phase PCC voltage will be obtained by the Park inverse transformation.

D. Partly Reactive Current Compensation Method in Case of the Inductive Load Connection

If only the positive-sequence fundamental reactive load current i_{Lqs} is compensated, then the steady component of the reactive component of a load current i_{Lqs} is used as the *q*-axis current reference of the LSC. That is

$$i_q^* = -i_{Lqs}. \tag{23}$$

So the steady reactive component in the stator PW current is zero, that is, $i_{spqs} = 0$. The drop of the PCC voltage Δu is

$$\begin{aligned}\Delta u_d &= R_{sp} i_{spds} + \frac{R_{sp}L - L_{sp\sigma}R}{L} i_{spdt} \\ \Delta u_q &= \omega L_{sp\sigma} i_{spds} + \frac{R_{sp}L - L_{sp\sigma}R}{L} i_{spqt}.\end{aligned} \tag{24}$$

According to (18), the drop of the PCC voltage Δu in phase-*a* is

$$\begin{aligned}\Delta u_a &= \sqrt{\left(R_{sp}^2 + \omega^2 L_{sp\sigma}^2\right) i_{spds}^2} \cos\left(\omega t + \varphi\right) \\ &\quad + \frac{R_{sp}L - L_{sp\sigma}R}{L} \left(i_{spdt} \cos\omega t - i_{spqt} \sin\omega t\right) \\ &= \frac{U_m}{|Z|} |Z_{sp}| \cos\phi \cos\left(\omega t + \varphi\right) \\ &\quad - \frac{U_m}{|Z|} \frac{R_{sp}L - L_{sp\sigma}R}{L} \cos\phi e^{-\frac{R}{L}t}.\end{aligned} \tag{25}$$

As shown in (25), the steady state of the voltage drop at the PCC has been decreased and the transient component is also the same as (18). So it is more stable than the control method with fully reactive current compensation.

From (23), it can be seen that only the steady-state component of the reactive load current i_{Lqs} is needed for this compensation method. This value can be obtained through the classic IRP theory and low-pass filter [22].

E. Simulation Results

The simulation is performed using the PLECS software to verify the performance and effectiveness of the proposed control. The configuration is given in Fig. 2. The parameters of the BDFIG system referred to the stator PW are listed in Table I.

The scalar control scheme is used for the BDFIG in the MSC control algorithm, shown in Fig. 3. The dynamic equivalent circuit for the BDFIG which is based on the two-axis model in the rotor reference frame is used as the simulation model. This dynamic equivalent circuit is described in [23]. The conventional method is used in design of the PI controller parameters [24]. In the double loop control of the LSC, the PI gain values of the inner current controller are $K_{ip} = 3$ and $K_{ii} = 400$. The PI gain values of the outer voltage controller are $K_{up} = 6$ and $K_{ui} = 300$.

TABLE I
PARAMETERS OF THE BDFIG SYSTEM

Symbol	Quantity	Value
S_N	Rated power	80 kVA
U_{sp}	Rated stator PW voltage	380 V
i_{sp}	Rated stator PW current	122 A
f_N	Rated operating frequency	50 Hz
p_p	Pole pairs of the stator PW	2
p_c	Pole pairs of the stator CW	4
ω_n	Natural speed	500 r/min
cosφ	Power factor	0.8
u_{dc}	DC-link voltage	700 V
f_s	Switching frequency	5 kHz
L_s	Filter inductance	0.209 p.u.
C_{dc}	DC-link capacitor	0.032 F
R_{sp}	Stator PW resistance	0.0428 p.u.
$L_{sp\sigma}$	Stator PW leakage inductance	0.214 p.u.
L_{spm}	Stator PW magnetizing inductance	19.187 p.u.
R_{sc}	Stator CW resistance	0.0405 p.u.
$L_{sc\sigma}$	Stator CW leakage inductance	0.116 p.u.
L_{scm}	Stator CW magnetizing inductance	5.03 p.u.
L_{rpm}	Rotor magnetizing inductance to the PW	19.223 p.u.
L_{rcm}	Rotor magnetizing inductance to the CW	5.035 p.u.
R_r	Rotor resistance	0.0573 p.u.
$L_{r\sigma}$	Rotor leakage inductance	0.0693 p.u.

After the BDFIG system is well settled, a sudden load from no load to a resistance–inductance load with the rated power of 80 kVA/380 V and the power factor of 0.6 is applied. The simulation results of the reactive current compensation method applied in LSC of the stand-alone BDFIG are given in Fig. 7.

Fig. 7(a) shows the transient responses of the PCC voltage without reactive current compensation in the LSC control. In this operation, the PCC voltage is compensated only by the MSC control. It can be seen that there is a large PCC voltage drop and slower dynamic performance. The main reason is that the bandwidth of the voltage loop in the MSC is narrow about 30 Hz. So the recovery time of the PCC voltage is long.

Fig. 7(b) shows simulation results of the PCC voltage with the fully reactive current compensation by the LSC. The PCC voltage contains numerous harmonic components and the transient time is very long. These harmonics harmfully affect the performance of other loads connecting to the PCC.

Fig. 7(c) shows the performance of the proposed control strategy for the steady component of the load reactive current compensation by the LSC. It can be seen that the quality of the PCC voltage is much more improved and can respond rapidly in case of the sudden load.

Using the simulation studies, it was shown that the transient reactive current compensation responses of a stand-alone system based on the BDFIG generator are satisfactory. This improves the dynamic performance of the control system.

As soon as the PCC voltage is in the steady state, the system control strategy is switched to the coordinated reactive power control scheme. The coordinator block calculates the desired

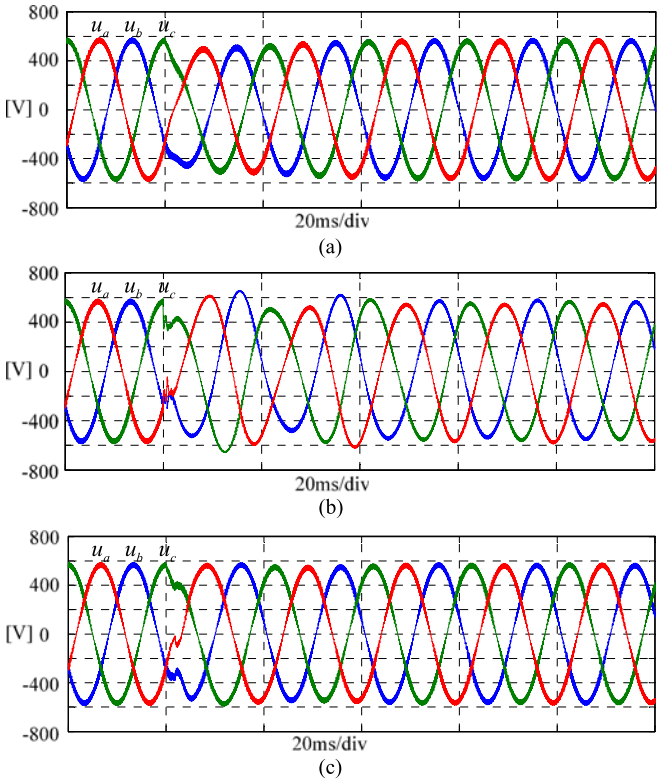

Fig. 7. Simulation results of the PCC voltage for three reactive current control methods: (a) PCC voltage without compensation, (b) PCC voltage with fully compensation, and (c) PCC voltage with partly compensation.

reactive power of the load and shares it to the LSC and MSC by changing the reactive power reference value of the controller, respectively. The strategy of allocation about the reactive power reference value is based on the outcome of the optimization problem [25].

IV. Transient Reactive Current Control After Sudden Load Disconnection

A. Reactive Current Control of the LSC During the Voltage Swell at the PCC

When the load is suddenly disconnected from the stator PW, the voltage swell at the PCC may be generated due to the abrupt interruption of the current. This voltage swell may cause the LSC uncontrollable due to the dc-link voltage limitation [26].

Under the PCC voltage-oriented reference frame, the voltage of the LSC in the synchronous *dq* axis reference frame can be expressed as [27]

$$U_m = R_s i_d + L_s \frac{di_d}{dt} - \omega L_s i_q + v_d$$
$$0 = R_s i_q + L_s \frac{di_q}{dt} + \omega L_s i_d + v_q \tag{26}$$

where L_s and R_s are the LSC filter inductance and inner resistance, respectively.

If neglecting the resistance R_s and operating under the unity power factor, the relationship of voltage space vectors of LSC

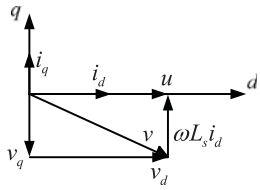

Fig. 8. Voltage space vector simplified diagram of the LSC.

in the steady state can be simplified as

$$v_d = U_m + \omega L_s i_q$$
$$v_q = -\omega L_s i_d. \tag{27}$$

The diagram is described as Fig. 8. Taking the principle of modulation into consideration, the maximum available LSC voltage has to be limited [24]

$$|v| = \sqrt{v_d^2 + v_q^2} \le \frac{u_{dc}}{m} \tag{28}$$

where m is the modulation index, and there is $m = 2$ for sinusoidal pulse width modulation and $m = \sqrt{3}$ for space vector pulse width modulation.

With (27) and (28), the lowest limit of the dc-link voltage of the LSC can be obtained as following expression

$$\sqrt{(U_m + \omega L_s i_q)^2 + (\omega L_s i_d)^2} \le \frac{u_{dc}}{m}. \tag{29}$$

Based on the (4), i_d will increase when the load becomes large. So from (29), the larger the load is, the higher the dc-link voltage is needed. Even at no-load situation, the dc-link voltage has the minimum value U_m which is the magnitude of the PCC voltage.

To simplify the analysis, the LSC is controlled to compensate all the reactive current produced by the inductive load. So in this steady-state situation, there is only active current i_{spd} in the stator PW of the stand-alone BDFIG and the reactive current i_{spq} is zero. Meanwhile, the main role of the MSC control is to regulate the magnitude of the PCC voltage as desired value U_m, so the active current of the load i_{Ld} can be expressed as

$$i_{Ld} = \frac{2}{3}\frac{P_L}{u_d} = \frac{2}{3}\frac{P_L}{U_m} \tag{30}$$

where P_L is the active power of the load.

When the load is suddenly disconnected from the stator PW, the load current is cut off. So $\Delta i_{spq} = i_{Ld}$. Then, the voltage swell at the PCC can be obtained based on (14)

$$\Delta u_d = R_{sp}\Delta i_{spd} + L_{sp\sigma}\frac{\Delta i_{spd}}{\Delta t} = \frac{2}{3}\frac{R_{sp}P_L}{U_m} + \frac{2}{3}\frac{L_{sp\sigma}P_L}{U_m \Delta t}$$
$$\Delta u_q = \omega L_{sp\sigma}\Delta i_{spd} = \frac{2}{3}\frac{\omega L_{sp\sigma}P_L}{U_m}. \tag{31}$$

It can be seen that when the load is larger, the voltage at the PCC swell higher.

The voltage of the LSC in *d*-*q* axis can be obtained when the load is suddenly disconnected from the PW

$$v_d = U_m + \omega L_s i_q + \Delta u_d$$
$$v_q = -\omega L_s i_d + \Delta u_q. \tag{32}$$

So the amplitude of the LSC voltage is

$$|v| = \sqrt{(U_m + \omega L_s i_q + \Delta u_d)^2 + (\omega L_s i_d - \Delta u_q)^2}. \quad (33)$$

When it is larger than u_{dc}/m, the LSC may be uncontrollable. As a result, to guarantee a safe operation of the LSC, the dc-link voltage which is controlled as a constant under normal operation may need to be increased.

From (33), we can see that it is effective to make the LSC output inductive reactive power, i.e., $i_q < 0$, in order to make the needed output voltage of the LSC less than that under the unity power factor operation and guarantee the normal operation of the BDFIG.

From (33), the following expression can be obtained:

$$i_q \le \frac{1}{\omega L_s}\left(\sqrt{\left(\frac{u_{dc}}{m}\right)^2 - (\omega L_s i_d - \Delta u_q)^2} - U_m - \Delta u_d\right). \quad (34)$$

So with this constraint of a reactive current of the LSC, the controllability of the LSC can be ensured, and the amplitude of the current i_q should be smaller than the maximum of the current $i_{\max}$ in the LSC.

However, the calculation is very complex based on (34), and the load current cannot be measured in case of sudden unload.

When the BDFIG is operating in the steady state, the following expression can be obtained based on (29):

$$\left(\frac{u_{dc}}{m}\right)^2 - (\omega L_s i_d - \Delta u_q)^2 > (U_m + \omega L_s i_q)^2 + 2\omega L_s i_d \Delta u_q - \Delta u_q^2. \quad (35)$$

Because Δu_q is usually very small compared to U_m, then

$$\left(\frac{u_{dc}}{m}\right)^2 - (\omega L_s i_d - \Delta u_q)^2 > U_m^2. \quad (36)$$

So the following formula can be obtained:

$$\sqrt{\left(\frac{u_{dc}}{m}\right)^2 - (\omega L_s i_d - \Delta u_q)^2} - U_m - \Delta u_d > U_m - \sqrt{\Delta u_q^2 + (U_m + \Delta u_d)^2}. \quad (37)$$

Then, the transient *q*-axis reference current i_q can be chosen as following for convenience according to (34):

$$i_q^* = \frac{k}{\omega L_s}(U_m - U'_m) \quad (38)$$

where U'_m is the instantaneous amplitude of the phase voltage at the PCC, and U_m is the rated value of the voltage. *k* insures that it does not exceed a maximum current $i_{\max}$ of the LSC.

With the regulation of the BDFIG system, the output voltage of the PW will be regulated to the rated value at the steady state. Then, i_q will return to the steady state. The LSC can be simply controlled in case of the voltage swell.

B. Transient Response of the DC-Link Voltage During Sudden Unload

Using (26), the relationship of voltage space vectors of LSC in the transient state can be obtained

$$\frac{di_d}{dt} = \frac{U_m - v_d + \omega L_s i_q}{L_s}. \quad (39)$$

With the above equation, it can be seen that if we want to guarantee the fastest transient response of the active current i_d, the rising and falling slopes of the active current i_d must be larger [28]. In (39), the U_m and L_s are the constant value. So the transient response of the active current depends on the voltage v_d and the reactive current i_q of the LSC.

When the load is disconnected from the stator PW, the *d*-axis reference current given by the outer loop voltage should decrease. The negative maximum voltage is required across the inductor L_s for the fast transient response and then the LSC voltage v_d should be changed into the positive maximum value. So the minimum possible time for tracking the reference current can be calculated as

$$\Delta T = L_s \frac{i_d^* - i_d}{v_{d\max} - \omega L_s i_q - U_m} \quad (40)$$

where $v_{d\max}$ is the maximum voltage generated by the LSC.

However, the maximum voltage $v_{d\max}$ is bounded as (28) if a PWM is used. So the value of $(v_{d\max} - \omega L_s i_q - U_m)$ is very small and ΔT becomes long. Therefore, if the *d*-axis reference current decreases, the current regulation is very slow due to the voltage constraint of the converter. This will make the dc-link voltage swell in a long transient period. Moreover, this phenomenon becomes more serious in the case of higher PCC voltage.

From (40), we can see that when the reactive current i_q becomes negative, the falling slope of the active current i_d becomes larger. Therefore, by utilizing the negative *q*-axis current, the less transient period is possible and the dc-link voltage can be fast tracking to the reference value.

The simulation of the HVRT control strategy of the LSC is shown in Fig. 9. The parameters of the system are the same in Table I.

When the load is suddenly disconnected from the stator PW, the swell of the voltage at the PCC will be generated shown in Fig. 9. Fig. 9(a) shows the normal operation of the LSC. It can be seen that the LSC fails to control the current and the dc-link voltage also exceeds the rating of the converter much more.

However, with the transient negative reactive current injected into the PCC according to (38), the LSC can remain controllable under the proposed HVRT control shown in Fig. 9(b). The transient response of the proposed current controller is much faster than that of the conventional PI regulator, and it is helpful to reduce the dc-link overvoltage.

V. Experimental Details

In order to verify the proposed control strategy, an 80kVA/380V stand-alone BDFIG system is constructed. The BDFIG is rotated by a 90kW three-phase asynchronous motor emulated as a prime mover with the speed control, shown

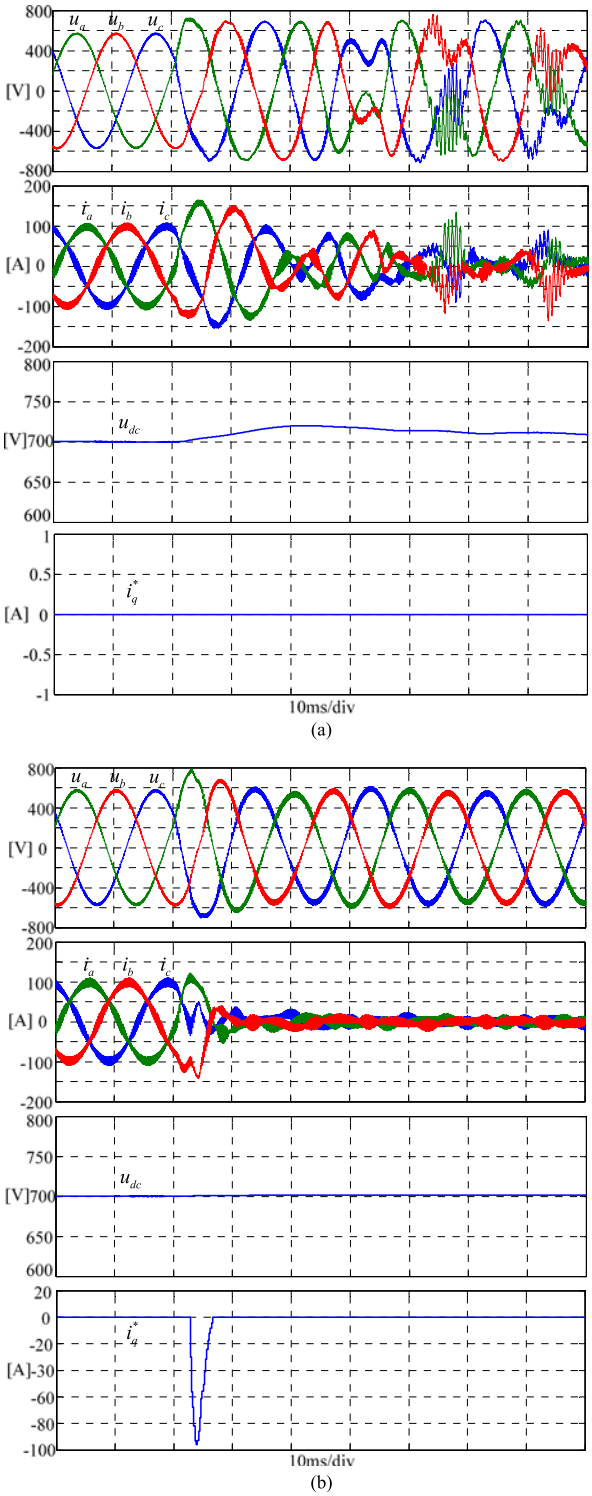

Fig. 9. Simulation results in case of the load disconnected from the PW: (a) traditional operation and (b) proposed HVRT control.

in Fig. 10(a). The control system is made up of the MSC and LSC, and the photograph is shown in Fig. 10(b). These two converters consist of a control board of 32-bit floating DSP TMS320F28335 of Texas Instrument, a power stage composed of six insulated-gate bipolar transistor with the switching frequency of 5 kHz and capacitors of the dc bus.

Fig. 10. Configuration of the experimental setup: (a) Prime mover and BDFIG system and (b) control system of the stand-alone BDFIG.

The experimental parameters are the same with the simulation listed in Table I.

For the sake of simplification, the rotor speed of the BDFIG is kept constant at subsynchronous value 400 r/min. After the system is well settled and the rotor speed is stable, a sudden resistance–inductance load with rated power of 80 kVA/380 V and the power factor of 0.6 is applied. The waveforms of the PCC voltage are given in Fig. 11.

Fig. 11(a) shows experimental results of the stator PW output voltage at the PCC without reactive current compensation method by the LSC. It can be seen that it has 18% of the voltage drop at the PCC. The reason is that the PCC voltage is controlled through regulating the stator CW current by the MSC indirectly. Since the BDFIG has a larger mechanical inertia, the change in the stator CW current will produce a certain delay through the

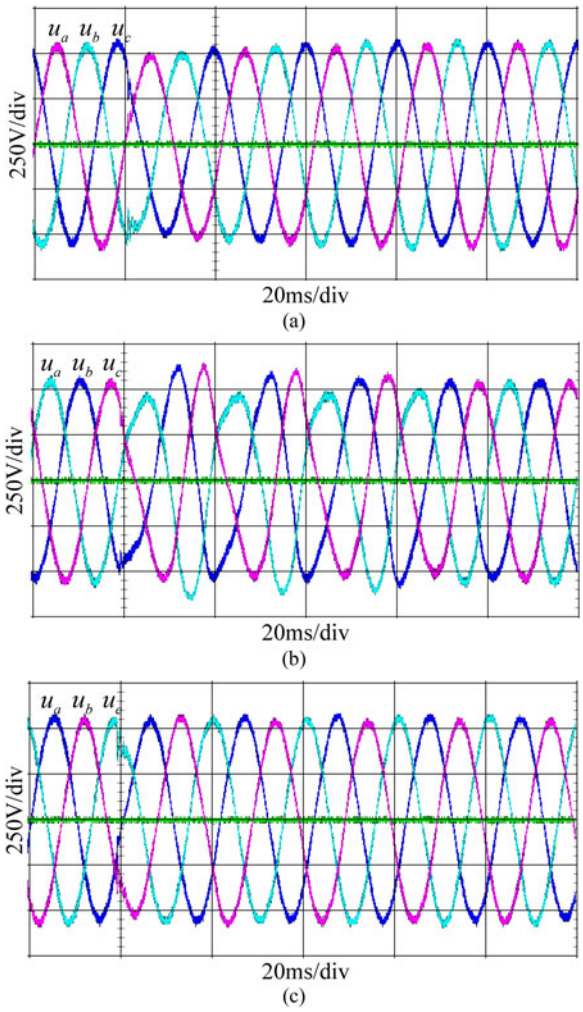

Fig. 11. Dynamic waveform when the resistance–inductance load connected at the PCC: (a) PCC voltage without compensation, (b) PCC voltage with fully compensation, and (c) PCC voltage with partly compensation.

rotor and stator PW of the BDFIG. Then, only with the stator CW current regulation by the MSC, the dynamic performance of the PCC voltage is slower and the transient time is long.

However, with the fully compensation method by the LSC, the voltage waveforms become distorted and unbalanced for a long time shown in Fig. 11(b). This is mainly because the decaying fundamental component in exponential form in the *d*-axis current is not compensated; this asymmetry of compensation causes the distortion at the PCC. If other loads are connected to the same PCC, their performance will be affected directly.

By adopting the proposed reactive current compensation method in the LSC, it can be seen that the PCC voltage can recover in one cycle which can be seen from Fig. 11(c). The quality of the PCC voltage is much more improved and can respond rapidly in case of the sudden load.

When the load is disconnected from the stator PW of the BDFIG, the waveforms of the dc-link voltage, the PCC voltage, and the current of the LSC are shown in Fig. 12.

Fig. 12(a) shows the normal operation without transient reactive current injected into the PCC. It can be seen that the voltage swell cause the LSC working abnormally. The oscillation occurs

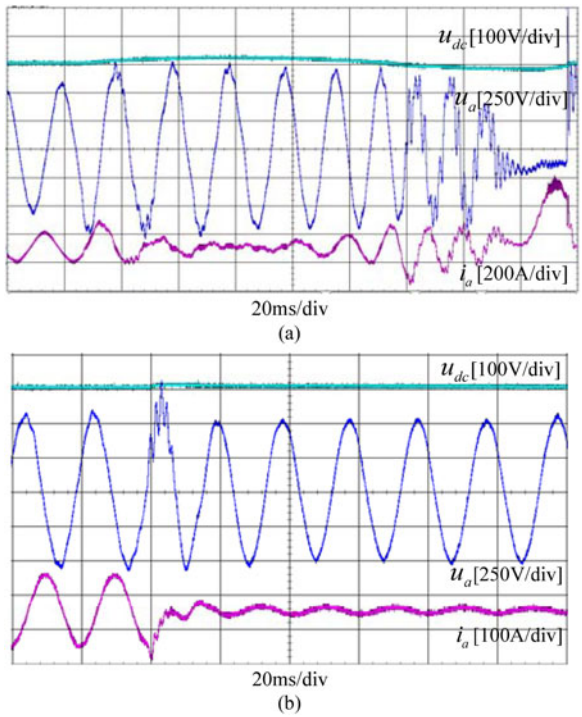

Fig. 12. Dynamic waveform when the resistance–inductance load disconnected from the PCC: (a) Normal operation and (b) HVRT control.

in *a*-phase current of the LSC and the dc-link voltage cannot be kept at the setting value.

In Fig. 12(b), with the proposed HVRT control method, the LSC has a higher capability to overcome grid voltage swell and significantly better transient performance. The current of the LSC becomes stable quickly and the peak value of the dc-link voltage is also reduced.

VI. Conclusion

This paper has proposed a transient reactive current control approach for a stand-alone BDFIG system to enhance the performance of the PCC voltage and the controllability of the LSC. The stator PW current and the voltage at the PCC are carried out when the resistance–inductance load is suddenly connected to the BDFIG. It results in the voltage drop and distortion at the PCC, and if only the positive-sequence fundamental reactive load current is used as the reference value of the *q*-axis current control loop in the LSC, the stator voltage can be significantly compensated. Another, the controllability of the LSC with limited rating considered during the PCC voltage swell is analyzed. A HVRT control strategy of the LSC is proposed by using the reactive current of the LSC, and it also improves the fast response the dc-link voltage in the transient region. The experimental results indicate that the compensation method performs well and can be used in practice.

References

[1] A. Zhang, X. Wang, W. Jia, and Y. Ma, "Indirect stator-quantities control for the brushless doubly fed induction machine," *IEEE Trans. Power Electron.*, vol. 29, no. 3, pp. 1392–1401, Mar. 2014.

[2] X. Chen, X. Wang, and F. Xiong, "Research on excitation control for stand-alone wound rotor brushless doubly-fed generator system," in *Proc. IEEE 2013 Int. Conf. Electr. Mach. Syst.*, 2013, pp. 663–667.
[3] F. Xiong and X. Wang, "Design and performance analysis of a brushless doubly-fed machine for stand-alone ship shaft generator systems," in *Proc. IEEE Electr. Contr. Eng. Conf.*, 2011, pp. 2114–2117.
[4] S. Shao, E. Abdi, F. Barati, and R. McMahon, "Stator-flux-oriented vector control for brushless doubly fed induction generator," *IEEE Trans. Ind. Electron.*, vol. 56, no. 10, pp. 4220–4228, Oct. 2009.
[5] V. E. Wagner, "Effect of harmonics on equipment," *IEEE Trans. Power Del.*, vol. 8, no. 2, pp. 672–680, Apr. 1993.
[6] K. Protsenko and D. Xu, "Modeling and control of brushless doubly-fed induction generators in wind energy applications," *IEEE Trans. Power Electron.*, vol. 23, no. 3, pp. 1191–1197, May 2008.
[7] M. Z. Sujod, I. Erlich, and S. Engelh, "Improving the reactive power capability of the DFIG-based wind turbine during operation around the synchronous speed," *IEEE Trans. Power Convers.*, vol. 28 no. 3, pp. 736–745, Sep. 2013.
[8] G. Y. Jeong, T. J. Park, and B. H. Kwon, "Line-voltage-sensorless active power filter for reactive power compensation," *IEE Proc. Electr. Power Appl.*, vol. 147 no. 5, pp. 385–390, Sep. 2000.
[9] V. T. Phan and H. H. Lee, "Control strategy for harmonic elimination in stand-alone DFIG applications with nonlinear loads," *IEEE Trans. Power Electron.*, vol. 26, no. 9, pp. 2662–2675, Sep. 2011.
[10] P. Verdelho and G. D. Marque, "DC voltage control and stability analysis of PWM-voltage-type reversible rectifiers," *IEEE Trans. Power Electron.*, vol. 45, no. 2, pp. 263–273, Apr. 1998.
[11] A. S. Yunus, A. Abu-Siada, and M. A. S. Masoum, "Application of SMES unit to improve the high-voltage-ride-through capability of DFIG grid connected during voltage swell," in *Proc. IEEE Innov. Smart Grid Technol. Asia*, 2011, pp. 1–6.
[12] M. N. Eskander and S. I. Amer, "Mitigation of voltage dips and swells in grid-connected wind energy conversion systems," in *Proc. ICROS-SICE Int. Joint Conf.*, 2009, pp. 885–890.
[13] C. Wessels and F. W. Fuchs, "High voltage ride through with FACTS for DFIG based wind turbines," in *Proc. 13th Eur. Conf. Power Electron. Appl.*, 2009, pp. 1–10.
[14] C. Feltes, S. Engelhardt, J. Kretschmann, J. Fortmann, F. Koch, and I. Erlich, "High voltage ride-through of DFIG-based wind turbines," in *Proc. IEEE Power Eng. Soc. Gen. Meet.*, 2008, pp. 1–8.
[15] C. J. Liu, X. B. Huang, M. Chen, and D. H. Xu, "Flexible control of dc-link voltage for doubly fed induction generator during grid voltage swell," in *Proc. IEEE Energy Convers. Congr. Expo.*, 2010, pp. 3091–3095.
[16] R. Li, R. Spee, A. K. Wallace, and G. C. Alexander, "Synchronous drive performance of brushless doubly-fed motors," *IEEE Trans. Ind. Appl.*, vol. 30, no. 4, pp. 963–970, Jul./Aug. 1994.
[17] V. T. Phan and H. H. Lee, "Performance enhancement of stand-alone DFIG systems with control of rotor and load side converters using resonant controllers," *IEEE Trans. Ind. Appl.*, vol. 48, no. 1, pp. 199–210, Jan./Feb. 2012.
[18] D. Zhou, R. Spee, and A. K. Wallace, "Laboratory control implementations for doubly-fed machines," in *Proc. IEEE Int. Conf. Ind. Electron. Contr. Instrum.*, 1993, pp. 1181–1186.
[19] B. V. Gorti, G. C. Alexander, and R. Spee, "Power balance considerations for brushless doubly-fed machines," *IEEE Trans. Energy Convers.*, vol. 11, no. 4, pp. 687–692, Dec. 1996.
[20] R. Pena, R. Cardenas, E. Escobar, J. Clare, and P. Wheeler, "Control system for unbalanced operation of stand-alone doubly fed induction generators," *IEEE Trans. Energy Convers.*, vol. 22, no. 2, pp. 544–545, Jun. 2007.
[21] C. Zhan, C. Fitzer, V. K. Ramachandaramurthy, A. Arulampalam, M. Barnes, and N. Jenkins, "Software phase-locked loop applied to dynamic voltage restorer (DVR)," in *Proc. IEEE Power Eng. Soc. Winter Meet.*, 2001, pp. 1033–1038.
[22] X. Wang, Z. Wang, and H. Lin, "A transient reactive current compensation for load-side converter of BDFIG in stand-alone operation," in *Proc. IEEE Energy Convers. Congr. Expo.*, 2015, pp. 1171–1177.
[23] R. Li, A. Wallace, and R. Spee, "Dynamic simulation of brushless doubly-fed machines," *IEEE Trans. Energy Convers.*, vol. 6, no. 3, pp. 445–452, Sep. 1991.
[24] X. Kong, Y. Yuan, P. Li, Y. Wang, and J. Lin, "The design and analysis of the PI regulator of three-phase voltage source PWM rectifier," in *Proc. IEEE Region 10 Conf. TENCON*, 2015, pp. 1–5.
[25] D. Wang, H. Wang, J. Jia, and Y. Zhang, "Reactive power control of doubly fed induction generator in wind farm under low grid voltage," in *Proc. IEEE Int. Conf. Crit. Infrastruct.*, 2010, pp. 1–6.
[26] H. W. van der Broeck, H. C. Skudelny, and G. V. Stanke, "Analysis and realization of a pulse width modulator based on voltage space vector," *IEEE Trans. Ind. Appl.*, vol. 24, no. 1, pp. 142–150, Jan./Feb. 1988.
[27] J. B. Hu and Y. K. He, "Modeling and control of grid-connected voltage sourced converters under generalized unbalanced operation conditions," *IEEE Trans. Energy Conv.*, vol. 23, no. 3, pp. 903–913, Sep. 2008.
[28] J. W. Choi and S.-K. Sul, "Fast current controller in three-phase AC-DC boost converter using d-q axis crosscoupling," *IEEE Trans. Power Electron.*, vol. 13, no. 1, pp. 179–185, Jan. 1998.

Xingwei Wang (S'12) was born in Hubei Province, China, in 1980. He received the B.S. and M.S. degrees in electrical engineering from Huazhong University of Science and Technology (HUST), Wuhan, China, in 2002 and 2005, respectively, where he is currently working toward the Ph.D. degree.

From 2005 to 2007, he was with Mindray Medical International Limited, Shenzhen, China, as a Research and Development Engineer. Since 2007, he has been with the College of Electrical and Electronic Engineering, HUST, where he is currently a Faculty Member. His research interests include matrix converter and ac motor drive.

Hua Lin (M'10) was born in Wuhan, Hubei Province, China, in 1963. She received the B.S. degree in industrial automation from Wuhan University of Technology, Wuhan, in 1984, the M.S. degree in electrical engineering from Naval University of Engineering, Wuhan, in 1987, and the Ph.D. degree in electrical engineering from Huazhong University of Science and Technology (HUST), Wuhan, in 2005.

From 1987 to 1999, she was in the Department of Electrical Engineering, Naval University of Engineering, as a Lecturer and Associate Professor. In October 2010, she was a Visiting Scholar with the Center for Advanced Power Systems, Florida State University, Tallahassee, USA. Since 1999, she has been with the College of Electrical and Electronic Engineering, HUST, where she became a Full Professor in 2005. She has authored or coauthored more than 50 technical papers in journals and conferences. She has been involved in the research and teaching in the field of power electronics and electric drive. Her research interests include high power, high-performance ac motor drives, and novel power converters and their control.

Prof. Lin has won twice the second-grade National Scientific and Technological Advance Prize of China in 1996 and 2003, respectively.

Zhe Wang was born in Shandong Province, China, in 1992. He received the B.S. degree in electrical engineering from China University of Mining and Technology, Xuzhou, China, in 2014. He is currently working toward the Ph.D. degree at Huazhong University of Science and Technology, Wuhan, China.

His current research interests include bidirectional ad/dc converter, modular multilevel converter, and energy storage system.